DOI: 10.61782/fa.2023.0315

forum acusticum 2023

TOWARDS AURALIZATION OF PASS-BY NOISE FROM RAILWAY WHEELS: SENSITIVITY TO THE LATERAL CONTACT POSITION

Jannik Theyssen*, **Astrid Pieringer**
Division of Applied Acoustics, Chalmers University of Technology, Gothenburg, Sweden

ABSTRACT

Railway rolling noise is typically described in equivalent pass-by noise levels. However, this descriptor does not always sufficiently correlate with the perceived annoyance of, for example, tonal components or transient effects. An auralisation of such effects allows researching this correlation. The wheels are a main contributor to the overall noise level above about 1 kHz. The low damping of the wheels leads to a strong modal behavior. Typically, modes with a strong axial response to a vertical excitation in the wheel-rail contact dominate the radiated sound. The lateral position of this contact point on the wheel tread, and thus the modal excitation, is therefore an important parameter in an auralisation. However, the exact contact location varies due to the lateral oscillation of the wheelset during running. This paper presents a computationally efficient, time-domain prediction model for the sound pressure produced by one wheel as it passes a stationary track-side position. The model makes use of pre-calculated acoustic transfer functions of each mode, which allow an evaluation of the modal contributions to the track-side sound pressure. The sensitivity of these modal contributions on the lateral contact position is analyzed.

Keywords: *railway noise, auralization, wheel modes*

1. INTRODUCTION

A passing railway wheel often produces a distinct piercing, metallic noise. This noise originates from the roughness-excited vibrations of the wheel, which are characterized by its strong modal behavior. Which modes contribute to the radiated noise depends, among others, on the contact position on the wheel. The modes of the wheel are similar to those of a circular disc, which Thompson [1] classifies based on their number of nodal diameters (κ), their number of nodal circles (m) and their main direction of motion (axial, radial, or circumferential): (κ, m, a/r/c). During rolling on straight track, the main direction of excitation at the wheel tread is radial. Since modes with strong axial motion on the wheel hub are comparatively good acoustic radiators, modes with a strong coupling between the radial direction at the tread to the axial direction on the hub are typically dominant noise sources [2].

Auralization describes the process of rendering a sound field from virtual sources [3]. Auralization of wheel/rail noise enables working with environmental noise problems in new ways compared to working with equivalent levels, opening up for investigating psychoacoustic metrics and intuitive communication with a broader public. Recent activities in this field include the SILENCE [4], TAURA [5] and SILVARSTAR [6] projects. In these models, the auralization is realized based on moving point sources. The source strength of these sources is estimated based on equivalent roughness spectra and transfer functions to the sound pressure.

An auralization of wheel noise requires knowledge about the modal contributions, since the wheel noise is dominated by its modes. The modal amplitude depends on the lateral excitation position of the wheel. In practice, this position is rarely known as it varies due to the natural variation of the running line, both on straight and curved track. It is unclear in how far the modal contribution to the total pressure signal during a pass-by changes with the lateral contact position and if this change is audible.

This paper describes an algorithm which allows the evaluation of the pass-by pressure signal of one wheel for

Corresponding author: *jannik.theyssen@gmail.com.*

each wheel mode. The model is then used to study the influence of the lateral contact position on the rolling contact force, the pass-by sound pressure level and the contribution of each wheel mode to the pass-by sound. The following Section 2 describes the modeling approach, introduces the wheel and track geometry and contact properties. Section 3 reports and discusses the results of the simulations related to the wheel/rail contact forces, the pass-by sound pressure, and the implications for an auralization of the signal. Section 4 concludes the article.

2. MODEL DESCRIPTION

The model used for the prediction of the sound radiation from railway wheels was developed in a recent doctoral thesis [7], using previous work by Pieringer [8] for the wheel/rail contact and interaction. The modelling approach consists of three main components, the wheel dynamics, the wheel / rail interaction, and the sound radiation, which are summarized below.

2.1 The wheel dynamics

The dynamic response of the wheel is modeled in a Finite Element approach, specifically the the waveguide FE method (WFEM) for curved waveguides [9–11]. The WFEM reduces the 3D domain formulation to multiple 2D problems by assuming harmonic oscillation around the circumference of the wheel. For each whole number of oscillations κ, the harmonic system of equations

$$\left[\mathbf{K}_2(-j\kappa)^2 + \mathbf{K}_1(-\mathrm{j}\kappa) + \mathbf{K}_0 - \omega^2\mathbf{M}\right]\mathbf{\Phi} = 0 \quad (1)$$

is solved. The variable κ is called the number of nodal diameters [2]. Solving the eigenvalue problem for each κ produces eigenfrequencies ω_l and mode shapes $\mathbf{\Phi}_l$ of the wheel. $\mathbf{K}$ and $\mathbf{M}$ are stiffness- and mass matrices. The variable ω is the angular frequency. The velocity field $\mathbf{v}$ on the wheel

$$\mathbf{v}(\mathbf{g}_c, \omega) = \sum_l A_l(\omega)\mathbf{\Phi}_l(\mathbf{g_c}) \quad (2)$$

is obtained by modal superposition. The modal amplitude A_l is

$$A_l(\omega) = \mathrm{j}\omega b_l(\omega)\mathbf{F}_e(\omega)\mathbf{\Phi}_l(\mathbf{g}_c) \quad (3)$$

with the point force $\mathbf{F}_e(\omega) = [F_\theta(\omega), F_y(\omega), F_r(\omega)]^T$ and the mode shape $\mathbf{\Phi}_l$ where $\mathbf{\Phi}_l(\mathbf{g})$ is a three element vector that contains the deflection of mode l at position $\mathbf{g}_c$ in circumferential, axial, and radial direction. The term

$$b_l(\omega) = \left(\Lambda_l(\omega_l^2 - \omega^2 + 2\mathrm{j}\omega\omega_l\zeta_l)\right)^{-1} \quad (4)$$

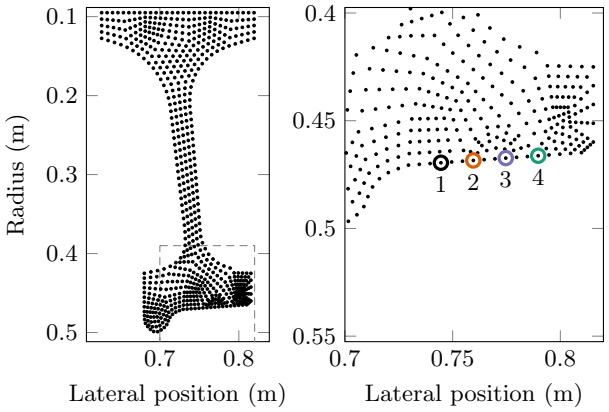

Figure 1. Wheel geometry, FE nodes and excitation positions 1 to 4.

describes the vibrational decay in the structure with the modal damping coefficient ζ_l, which is 10^{-3} for $\kappa = 0$, 10^{-2} for $\kappa = 1$, and 10^{-4} for $\kappa \leq 2$ (cf. [2]), and the modal mass

$$\Lambda_l = \mathbf{\Phi}_l^{\mathrm{T}}\mathbf{M}\mathbf{\Phi}_l \, . \quad (5)$$

The prediction of the wheel structural response serves two purposes: One, the velocity field is input to the sound radiation module, and two, the receptance at the rolling point on the wheel is needed for the prediction of the wheel/rail interaction. From this receptance, displacement impulse response functions are calculated by inverse Fourier transform. The rigid body modes of the wheelset are included in the wheel model for the prediction of the contact forces.

In the following, a reprofiled wheel of type BA093 with a rolling radius of 0.469 m is used as the geometry. A detailed modal analysis of this wheel is carried out in [7, 11]. The cross-section is discretized into 146 quadrilateral 9-node elements. The FE-nodes are shown in Fig. 1, of which four are used to investigate the effect of different lateral contact positions on the radiated sound pressure. These are located laterally 6.4 cm, 7.9 cm, 9.4 cm, and 10.9 cm from the flange back, respectively.

Fig. 2 shows the point mobility at each of these nodes. Notice the large dynamic range due to the lightly damped modes. Changing the contact node can change the magnitude of the resonances and the location of the anti-resonances for some modes. This is due to the different radial deflection at the different nodes in each mode shape. Fig. 3 shows these radial deflections for the four modes highlighted in Fig. 2. The mobility of the first mode (4,

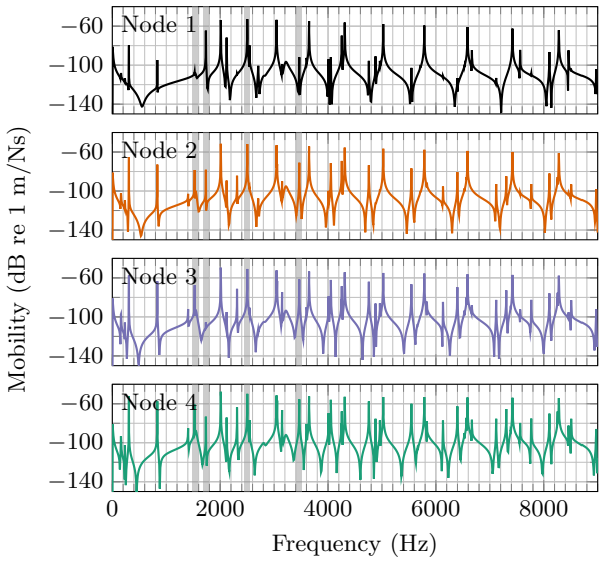

Figure 2. Predicted radial point mobility at each contact point. The four highlighted resonances belong to the modes (4, 0, a), (2, 1, a), (3, 0, r), and (3, 2, a), sorted by increasing frequency.

0, a) has a small resonance peak for excitation at Node 1, which increases for excitation positions towards Node 4 due to the increasing radial response. Analogous relations are observable for the other modes and contact nodes.

2.2 The wheel/rail interaction

The interaction between the wheel and the track is calculated in the time domain using moving Green's functions [12, 13]. This time-domain approach allows including the nonlinear behavior in the contact patch. The contact area is discretized and at each time step, Kalker's variational method [14] is used to solve the normal contact problem. A three-dimensional profile of wheel and rail roughness is considered. The tangential wheel/rail interaction and contact can be included [13] but have been neglected here. The rotation of the wheel is neglected.

For this example, a pass-by with the vehicle speed of 100 km/h is simulated. A track consisting of rails with a UIC60 E2 profile on monobloc concrete sleepers in ballast is modeled with finite elements in DIFF [15]. The track parameters are listed in [16]. The used track surface roughness is a measured roughness from a high-speed line in Germany [17]. A surface roughness measurement on a wheel with composite brake blocks [18] serves as the input to the wheel model. Average spectra of the wheel and rail roughness are shown in Fig. 4.

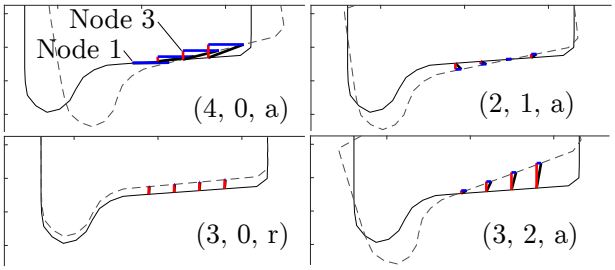

Figure 3. Wheel tread motion at four eigenmodes. The radial and axial displacement at the four excitation nodes are indicated with red and blue lines, respectively.

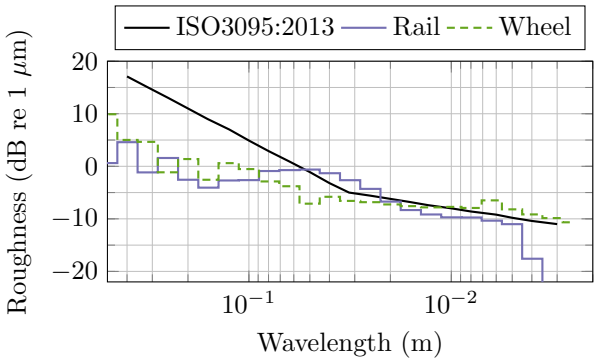

Figure 4. Average wheel and rail roughness spectra, in one-third octave bands.

2.3 The sound radiation

The Fourier series Boundary Element method (FBEM) [11, 19] is used to calculate the sound radiated by each wheel mode l for a stationary wheel. The sound pressure is evaluated on a sphere with 5 m radius around the wheel center. In a second step, the sound field of each mode is decomposed into spherical harmonics (SH) equivalent sources. This has the advantage that sound pressure transfer functions $H_l(\Delta\mathbf{x}, \omega)$, $\Delta\mathbf{x} = \mathbf{x}_{\text{Receiver}} - \mathbf{x}_{\text{Source}}$, can be efficiently calculated for any receiver position in 3D space [7]. These transfer functions describe the sound pressure at a receiver point that the wheel mode l produces at unit modal amplitude. During rolling of the wheel on the rail, this

modal amplitude varies due to the vibrational decay in the wheel and the varying modal excitation. The decay, corresponding to the term $b_l(\omega)$ in (3) can be expressed analytically in time domain

$$b_l = \frac{\mathrm{e}^{-2\omega_l \zeta_l t}}{\Lambda_l \omega_l'} \sin \omega_l' t \mathrm{H}(t) \tag{6}$$

with the Heaviside function $\mathrm{H}(t)$. The modal excitation becomes

$$F_{A,l}(t) = \frac{\mathrm{d}}{\mathrm{d}t} \mathbf{F}_\mathrm{e}(t) \mathbf{\Phi}_l(\mathbf{g_c}) \tag{7}$$

when expressed in the time domain. Convolution of $b_l(t)$ and $F_{A,l}(t)$ produces a quantity $q_{\mathrm{S},l}(t)$

$$q_{\mathrm{S},l}(t) = \int_{-\infty}^{t} F_{A,l}(\tau) b_l(t-\tau) \mathrm{d}\tau \tag{8}$$

which describes the amplification of each mode at each time step, taking into account the history of all contact forces and the dynamic response of the mode. Inverse Fourier transform of $H_l(\Delta\mathbf{x}, \omega)$, produces impulse response functions $h_l(\Delta\mathbf{x}, t)$ of the pressure signal due to unit modal excitation. Convolution of $q_{\mathrm{S},l}$ and h_l then allows calculating the pass-by pressure at a stationary receiver position of mode l

$$p_l(0, y_0, z_0, t) = \int_{-\infty}^{t} q_{\mathrm{S},l}(\tau) h_l(v\tau, t-\tau) \mathrm{d}\tau \tag{9}$$

The computational advantage of this modal approach is that the acoustic propagation functions $H_l(\omega)$ are rather smooth, so they can be evaluated with a broad frequency spacing in the BE solution. The total pressure is then calculated as the sum of all modal contributions.

3. RESULTS

3.1 Differences in the rolling contact force

The wheel/rail interaction is influenced by the lateral contact position. The large mobility at wheel resonances typically leads to a reduced rolling contact force at this frequency (similar to the low force that is needed to deflect a soft spring). Analogously, large rolling contact forces are expected at the anti-resonances. This is visible in the spectrum of the rolling contact forces around the mode (3, 2, a) in Fig. 5, where the dip at 3460 Hz marks the resonance, while the frequency of the anti-resonance changes with the excitation position.

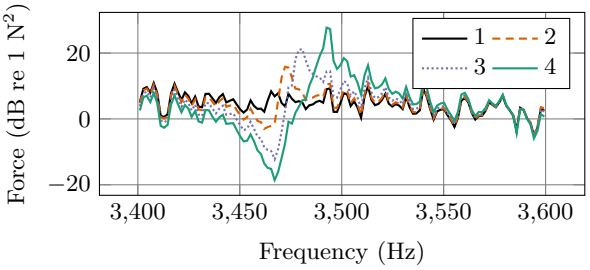

Figure 5. Effect of moving the contact position on the contact force spectrum around the mode (3, 2, a).

Table 1. Predicted total pass-by pressure levels of a single wheel.

Node 1	Node 2	Node 3	Node 4
60.6 dB	64 dB	66.7 dB	69.5 dB

Fig. 6 presents the frequency spectrum of the rolling contact force for Node 1. Sharp dips mark the position of modes with high radial mobility at the contact point. The other results are presented as relative differences to the first node. Large differences of up to 20 dB are observable for specific modes, many of which are axial modes. One such example is the mode (3, 2, a) (cf. Fig. 3 and Fig. 5), which is more readily excited due to its increasing radial component towards the outer excitation positions. The four highlighted regions mark the location of the modes described above.

3.2 Differences in the modal contribution to the pass-by pressure

The pass-by pressure is evaluated for each mode in a standard receiver position at $y = 7.5$ m distance from the track center, $z = 1.2$ m above the rail. The predicted total sound pressure level is then calculated by summing over the modal contributions. A sound pressure level increase of 9 dB is predicted when changing the excitation position from Node 1 to Node 4, as presented in Tab. 1. A possible reason for this large increase could be the neglected lateral interaction in the contact point, which leads to an overestimation of the contribution of the axial modes [2, 20]. Audio examples of the sound pressure signals for the various excitation positions are available online [21]. Fig. 7 shows the sound pressure level of excitation nodes 2 to 4 relative to Node 1 in third-octave bands. In general, the

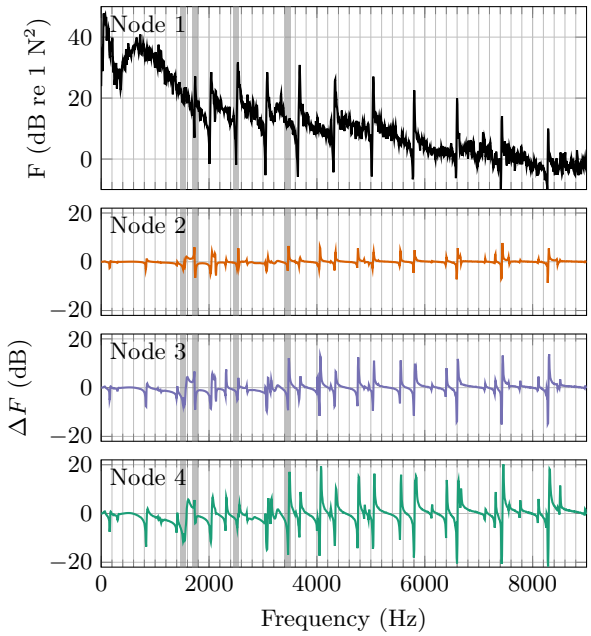

Figure 6. Power spectrum of the rolling contact forces for Node 1, and the spectra for Node 2 – 4 normalized with Node 1. Modes highlighted as in Fig. 2. The spectrum has a resolution of 6.8 Hz.

outer excitation position corresponds to higher levels.

To analyze the differences in the third-octave bands, the modal contributions to the total sound radiation are investigated. An equivalent sound pressure level $L_{\mathrm{p,eq,1s}}$ of each mode during 1 s of the pass-by is calculated. As 1 s corresponds to about 28 m traveling distance, the pressure level is averaged for wheel positions between about $x = -14$ m to 14 m. The $L_{\mathrm{p,eq,1s}}$ of each wheel mode is compared in Fig. 8 for two excitation nodes, Node 1 and Node 3. The modes are arranged in the dispersion diagram of the wheel [7, 11], where the different mode types are indicated by marker shapes. Connected modes share the same number of nodal circles. The largest increase is observable for axial modes, specifically axial modes with 2 and three nodal circles above about 5 kHz and the modes (4, 0, a), (5, 0, a) and (0, 1, a). The largest decrease is observed for the radial mode (1, 0, r) and the axial mode (2, 1, a). These differences are to a large degree explained by the difference in the point mobilities.

However, a large increase in the equivalent pressure level does not necessarily mean that the mode is more relevant to the absolute sound pressure at a stationary receiver position. In fact, it is found that the contribution of most modes can be removed from the total pressure signal without affecting the total sound pressure level. To show this, an analysis is carried out in which modal contributions are iteratively removed. In each iteration, the mode with the least significant contribution to the total level is determined by removing each modal contribution and evaluating the level differences to the previous total pressure level. Then, the contribution of the mode with the smallest level difference is removed and a new, temporary total level L^- is calculated by summation of the remaining modal contributions. By iteration through all included modes, the modes are sorted by least to most significant. Fig. 9 shows the level differences between the level L^- and the initial pressure level L_0. According to this calculation, more than 50 of the 58 considered modes can be removed with an error not exceeding 0.5 dB.

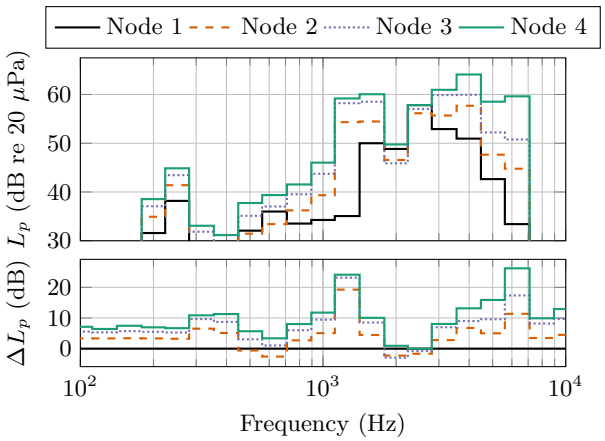

Figure 7. Total sound pressure level and level for excitation at nodes 2 to 4 normalized to Node 1.

Identifying modes significant to the equivalent sound pressure level can be relevant for, for example, designing noise mitigation measures. Fig. 10 shows the highlighted section in Fig. 9. The most significant modes for the prediction of the sound pressure level can be identified. The six modes that together produce a sound pressure level within 1 dB of the total level are also indicated in Fig. 8. For an excitation at Node 1, five modes produce a sound pressure level within 1 dB of the total, which are likewise indicated in Fig. 8. There is a partial overlap between the sets of significant modes for both excitation positions at the modes (3, 2, a) and (4 1, a). These modes could, for example, be targeted for noise mitigation measures. Identifying significant modes for an auralization of the pass-by

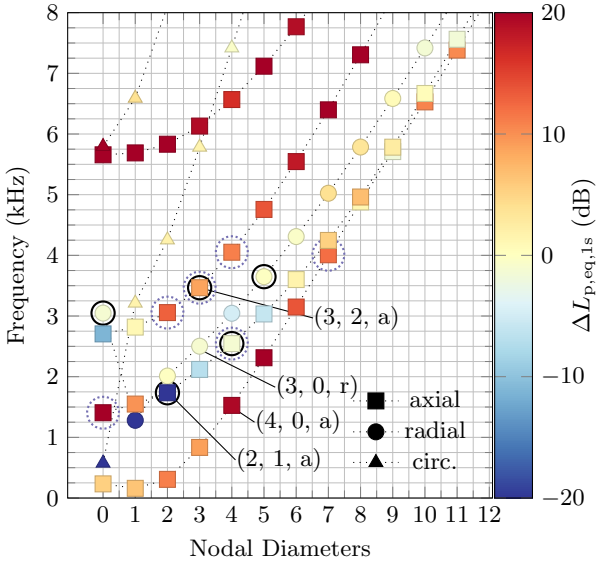

Figure 8. Dispersion diagram where each marker represents a mode of the wheel. The color indicates the difference in $L_{p,eq,1s}$ between excitation at Node 1 and Node 3, where positive differences correspond to larger radiation for an excitation at Node 3. Modes marked with black (○) and blue dotted (◌) circles are the identified 'significant modes' for excitation at Node 1 and Node 3, respectively.

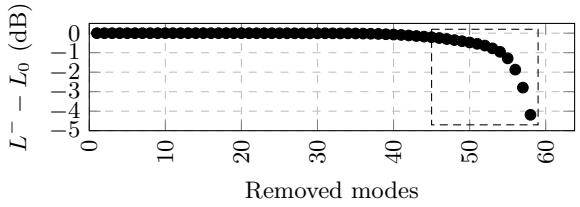

Figure 9. Iterative removal of modal contribution to the total sound pressure: pressure level difference of the remaining modes L^- compared to the initial pressure level L_0. Excitation at Node 3.

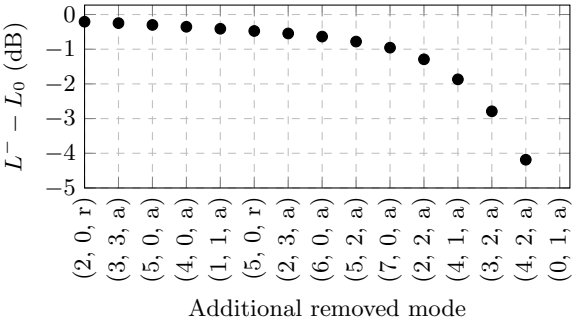

Figure 10. Section of Fig. 9, with labelled modes.

signal is not as simple, which is discussed below.

3.3 Towards auralization

The analysis above shows that a limited number of modes is relevant for producing the total sound pressure level, and that this set of modes changes for different excitation positions. However, for an auralization of the signal, the authors' experience is that considerably more than just the set of 'significant modes' need to be included before no difference is audible between the original signal and the signal with reduced number of modes. This is to a large degree due to the tonal characteristic of the wheel modes. The absence of several modes outside of the set of 'significant modes' is easily detectable aurally. Audio examples are provided online [21]. Classifying modes as significant for auralization, possibly depending on the lateral excitation position, would require listening experiments, which have not been carried out.

With the primary goal of auralizing the pass-by sound of a whole train, producing a realistic audio representation of iterative pass-bys of individual wheels is a key element. Based on the experience of the authors, assigning identical pressure signals to each wheel leads to a audio signal that seems artificial due to the exact repetition in the signal. In reality, the contact point varies due to variations the running line occuring both on curved and straight track. Several other factors influence wheel radiation, such as the geometry, the profile of the running surface, and the surface roughness. Here, the presented algorithm is used to generate time signals of pass-bys for eight consecutive wheels in four bogies of three coaches (including the second bogie of the first coach and the first bogie of the third coach). The combined roughness is assumed to be identical. The distances between the wheels are only approximated for this demonstration: the distance between two wheelsets in a bogie is 2.5 m, the distance between two bogies is 10 m, and the distance between two bogies on a single coach is 20 m. The two spectrograms in Fig. 11 show the pass-by sound pressure in a stationary, track side position 7.5 m beside the track. Audio examples are provided on-

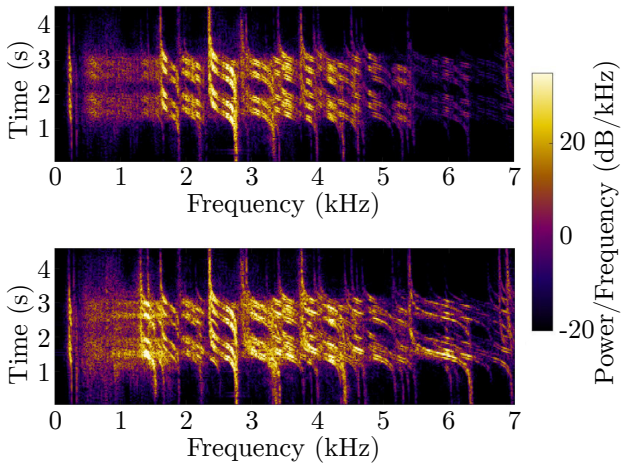

Figure 11. Spectrograms of pass-bys of four consecutive bogies. Top: identical noise signal for all eight wheels, bottom: varying contact position.

line [21]. The identical contact position for all wheels in the first signal leads to the repetitive pattern. In the second signal, a varying contact position is prescribed, arbitrarily assigning the four pass-by signals generated above to the eight wheels. The temporal variation of the pattern is most visible in the frequency region above 5 kHz, where a strong dependency of the modal contributions on the contact position was observed (cf. Fig. 8). Evaluating which of the signals is perceived more realistic requires conducting listening tests, which have not been carried out yet. Nevertheless, some variation of the radiation from each wheel is to be expected due to the varying lateral contact position, varying wheel geometry, wheel roughness, and possibly other surface defects such as wheel flats.

4. SUMMARY AND CONCLUSIONS

A time-domain model for predicting pass-by rolling noise from railway wheels is presented. The modeling approach uses Finite Element and Boundary Element methods to predict the modes of the wheel and the radiation from each mode. The sound field produced by each mode is represented in a spherical harmonics formulation, which facilitates the calculation of acoustic impulse responses describing the pressure response at a track side position for any position of the wheel. By describing each modal amplitude in the time domain, an efficient prediction of the pass-by pressure signal is achieved.

This paper investigates the influence of the wheel's lateral contact position in four different positions. Large differences in the contact force are observed for different contact positions. These differences are explained by the modal behavior of the wheel which affects the relevant point mobility, leading to dips and peaks in the contact force spectrum at resonances and anti-resonances, respectively. An increase of up to 9 dB is observed in the equivalent sound pressure level between the lateral contact positions. A possible explanation is that lateral interaction was neglected in the rolling contact, which can lead to an overestimation of the contribution of the axial modes. Comparing frequency spectra of the equivalent sound pressure level showed the highest levels for the node furthest from the flange. The increase is different across the frequency spectrum, depending on the level of excitation of each mode. Analyzing the contribution of each mode to the pass-by pressure showed a strong dependency on the contact position. Further, it was observed that only contributions from few (here four to six) modes are needed to predict the sound pressure level to within 1 dB error. This set of modes significant to the sound pressure level varies between lateral positions.

Working towards an auralization, two sets of pass-by predictions were calculated and evaluated by the authors. It is found that the set of modes identified in the previous analysis is insufficient to recreate the sound signal with all modes included. Further, for multiple wheels passing by a stationary observer, a variation in the lateral contact position of the wheel can lead to a more realistic combined sound signal due to decreased repetitiveness. Listening tests are necessary to quantify the latter results. Audio examples are available online [21]. This model would need to be complemented with the rail and sleeper contribution to fully capture rolling noise.

5. ACKNOWLEDGMENTS

The current study is part of the ongoing activities in CHARMEC – Chalmers Railway Mechanics (www.charmec.chalmers.se).

6. REFERENCES

[1] D. Thompson and C. Jones, "Sound radiation from a vibrating railway wheel," *JSV*, vol. 253, no. 2, pp. 401–419, 2002.

[2] D. J. Thompson, *Railway noise and vibration: mechanisms, modelling and means of control*. Amster-

dam ; Boston: Elsevier, 1st ed ed., 2009. OCLC: ocn245558640.

[3] M. Kleiner, B.-I. Dalenbäck, and P. Svensson, "Auralization-An Overview," *AES*, vol. 41, no. 11, pp. 861–875, 1993.

[4] E. Bongini, S. Molla, P. E. Gautier, D. Habault, P. O. Mattéi, and F. Poisson, "Synthesis of Noise of Operating Vehicles: Development within SILENCE of a Tool with Listening Features," in *Noise and Vibration Mitigation for Rail Transportation Systems* (B. Schulte-Werning, D. Thompson, P.-E. Gautier, C. Hanson, B. Hemsworth, J. Nelson, T. Maeda, and P. de Vos, eds.), Notes on Numerical Fluid Mechanics and Multidisciplinary Design, (Berlin, Heidelberg), pp. 320–326, Springer, 2008.

[5] R. Pieren, K. Heutschi, J. M. Wunderli, M. Snellen, and D. G. Simons, "Auralization of railway noise: Emission synthesis of rolling and impact noise," *Appl. Acoust.*, vol. 127, pp. 34–45, 2017.

[6] R. Pieren, F. Georgiou, D. Thompson, K. Heutschi, G. Squicciarini, M. Rissmann, and P. Bouvet, "Silvarstar - Soil Vibration and Auralisation Software Tools for Application in Railways. Deliverable D4.1: Methodology for auralisation adn virtual reality of railway noise.," tech. rep., European Commission, 2021.

[7] J. Theyssen, *Simulating rolling noise on ballasted and slab tracks: vibration, radiation, and pass-by signals*. Doctoral Thesis, Chalmers University of Technology, Gothenburg, Sweden, 2022.

[8] A. Pieringer, W. Kropp, and D. J. Thompson, "Investigation of the dynamic contact filter effect in vertical wheel/rail interaction using a 2D and a 3D non-Hertzian contact model," *Wear*, vol. 271, no. 1, pp. 328–338, 2011.

[9] S. Finnveden and M. Fraggstedt, "Waveguide finite elements for curved structures," *JSV*, vol. 312, no. 4-5, pp. 644–671, 2008.

[10] P. Sabiniarz and W. Kropp, "A waveguide finite element aided analysis of the wave field on a stationary tyre, not in contact with the ground," *JSV*, vol. 329, no. 15, pp. 3041–3064, 2010.

[11] F. Fabre, J. S. Theyssen, A. Pieringer, and W. Kropp, "Sound radiation from railway wheels including ground reflections: A half-space formulation for the fourier boundary element method," *JSV*, vol. 493, p. 115822, 2021.

[12] A. Pieringer, *Time-domain modelling of high-frequency wheel/rail interaction*. Doctoral Thesis, Chalmers University of Technology, Gothenburg, Sweden, 2011.

[13] A. Pieringer, W. Kropp, and J. C. O. Nielsen, "The influence of contact modelling on simulated wheel/rail interaction due to wheel flats," *Wear*, vol. 314, no. 1, pp. 273–281, 2014.

[14] J. J. Kalker, *Three-Dimensional Elastic Bodies in Rolling Contact*, vol. 2 of *Solid Mechanics and Its Applications*. Dordrecht: Springer Netherlands, 1990.

[15] J. Nielsen and A. Igeland, "Vertical dynamic interaction between train and track influence of wheel and track imperfections," *JSV*, vol. 187, no. 5, pp. 825–839, 1995.

[16] A. Pieringer and W. Kropp, "Model-based estimation of rail roughness from axle box acceleration," *Appl. Acoust.*, vol. 193, p. 108760, 2022.

[17] D. Thompson, G. Squicciarini, J. Zhang, I. Lopez Arteaga, E. Zea, M. Dittrich, E. Jansen, K. Arcas, E. Cierco, F. X. Magrans, A. Malkoun, E. Iturritxa, A. Guiral, M. Stangl, G. Schleinzer, B. Martin Lopez, C. Chaufour, and J. Wändell, "Assessment of measurement-based methods for separating wheel and track contributions to railway rolling noise," *Appl. Acoust.*, vol. 140, pp. 48–62, 2018.

[18] V. Delavaud, *Modélisation temporelle de l'interaction roue/rail pour une application au bruit de roulement ferroviaire*. Doctoral Thesis, ENSTA ParisTech, 2011.

[19] A. H. W. M. Kuijpers, G. Verbeek, and J. W. Verheij, "An improved acoustic Fourier boundary element method formulation using fast Fourier transform integration," *JASA*, vol. 102, no. 3, pp. 1394–1401, 1997.

[20] G. Cheng, Y. He, J. Han, X. Sheng, and D. Thompson, "An investigation into the effects of modelling assumptions on sound power radiated froma high-speed train wheelset," *JSV*, vol. 495, p. 115910, Mar. 2021.

[21] J. Theyssen, "Complementary files to the publication 'towards auralization of pass-by noise from railway wheels: sensitivity of the lateral contact position'." http://www.ta.chalmers.se/research/vibroacoustic-group/audio-examples/fa2023a/.